IEEE Access
Multidisciplinary | Rapid Review | Open Access Journal

SPECIAL SECTION ON RADIO FREQUENCY IDENTIFICATION AND SECURITY TECHNIQUES

Received November 1, 2018, accepted November 21, 2018, date of publication December 3, 2018,
date of current version December 27, 2018.

Digital Object Identifier 10.1109/ACCESS.2018.2883439

A High Gain Dual Polarized Ultra-Wideband Array of Antenna for Chipless RFID Applications

FATEMEH BABAEIAN, (Student Member, IEEE), AND NEMAI CHANDRA KARMAKAR, (Senior Member, IEEE)

Department of Electrical and Computer Systems Engineering, Monash University, Melbourne, VIC 3800, Australia

Corresponding author: Fatemeh Babaeian (fatemeh.babaeian@monash.edu)

This work was supported by the Australian Research Council Link Project: Discreet Reading of Printable Multi-Bit Chipless RFID Tags on Polymer Banknotes under Grant LP130101044.

ABSTRACT In this paper, an ultra-wideband, orthogonally polarized, and high-gain microstrip patch antenna array with 8 × 8-element for the chipless radio frequency identification (RFID) applications is proposed. This planar-structure antenna has a high front-to-back ratio in a wide frequency band. The element comprises an interleaved aperture-coupled dual polarized stacked microstrip patch antenna with air gaps and complementary back reflectors. The stacked patch elements are etched on Taconic TLX-8 substrate and the complementary back reflectors are etched on FR-4. The presence of back reflectors reduces the back-lobe level significantly. The antenna array operates over 4.2–7.1 GHz and yields 26-dBi gain. Overall, the antenna yields 51.3% fractional bandwidth centred at 5.65 GHz. The antenna can read a multi-bit chipless RFID at a distance of 8 m with a transmit power of −10 dBm.

INDEX TERMS Aperture coupled microstrip patch antenna, antenna array, ultra-wideband (UWB), bandwidth, gain, reflection coefficient, polarisation, chipless RFID, tag detection.

I. INTRODUCTION

Radio frequency identification (RFID) is a wireless data transmission and reception technology for tracking and identification. RFID systems consist of three main elements: a transponder or RFID tag for carrying identification code, an integrator for sending signals to RFID tag, receiving the scattered signal and identifying the ID, and middleware software which maintains an interface to encode identification data from the reader to a personal computer [1].

Chipped RFID systems have been developed since the last century and are one of the most popular techniques for automatic identification, access control, tracking and tracing. However, the tag is Application Specific Integrated circuit (ASIC) chip which is expensive. The ASIC chip makes the tag non-planar and hence it cannot be printed on items such as a barcode. The alternative solution to this problem is the chipless RFID system. A chipless tag is a fully passive microwave circuit and can be printed on paper and plastic. Therefore, the low price of printed tag beside the non-line of sight detection aspect makes this technology competitive with the available optical barcode in the market [2]. The chipless RFID system comprises a UWB reader, UWB antenna, and passive chipless RFID tags.

The chipless RFID system uses a backscattering tag that contains distinct frequency signatures. The reading range is limited to a few centimetres due to the UWB low transmit power regulation. The reading range of the chipless RFID system is a function of the tag's radar cross section (RCS), the reader's sensitivity and the reader antenna performance. For a specific tag and a reader, the reading range is limited to the gain of the antenna, angular beam width for covering the reading zone and the matching condition of the antenna. Fig1 illustrates a chipless RFID system. As can be seen, the reader sends a UWB transmit signal with uniform amplitude to illuminate the tag. The tag in return sends the echo with discrete frequency signatures (resonances/dissonances) to the reader. The reader antenna receives the signal and the receiver process the tag ID.

Since chipless RFID systems operate as an ultra-wideband system, designing a UWB high gain reader antenna is very crucial. The main challenge in designing an antenna for chipless RFID applications is to provide high gain over ultra-wide

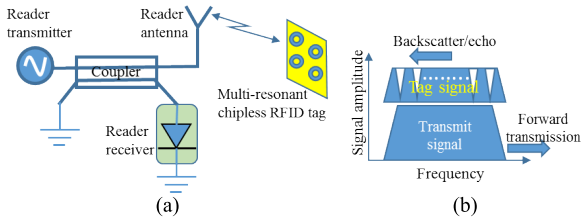

FIGURE 1. (a) Chipless RFID system, (b) signal spectrum.

bandwidth with low return loss. Moreover, in applications, in which tag detection is in the near field of the antenna, it is demanded to produce uniform illumination of the reading zone with the aid of array synthesis and beam shaping techniques.

In literature, a few types of the antenna were reported for chipless RFID applications. The first one is a circular disk-loaded monopole antenna which has a wide band (3-11GHz) and low gain (near 0 dB) with an omnidirectional pattern [3], [4]. The low gain in this structure caused the limitation in the reading range for chipless RFID tag detection. Also, an elliptical leaf dipole was introduced in [5], which had a wide bandwidth, between 4-6 GHz, and maximum gain of 15 dBi in array form of 2∗2 elements. The drawbacks of this structure were having bulky and non-planar structure, which required complex soldering and assembly techniques. The other introduced UWB antenna for chipless RFID application was a log periodic dipole antenna which had a gain of 7.3 dBi [5]. Although this antenna had a wide bandwidth, the non-planar structure in array form and its massive size caused difficulties in the manufacturing process and implementing in systems in which a planar reader structure is required. In [6], an aperture excited patch antenna, which operated at 6.8-11 GHz and had a maximum gain of 7dBi, was introduced. Due to the planar radiation pattern of this antenna, this structure is a convenient design for chipless RFID tag detection, but there was a drawback of high back lobe level in the radiation pattern.

The high back lobe level in an antenna causes high sensitivity to the noise in the environment for chipless RFID tag detection. The reason behind this phenomenon is that in chipless RFID system, it is desired to measure the RCS of the tag, which is placed at the front of the reader antenna. In the case having a high back lobe level in the reader antenna, the loading effect of items behind the reader antenna could cause interference in the measured signal. This problem can be significant when the tag RCS is being measured in motion. Therefore, reducing the back lobe level of the antenna is very crucial for chipless RFID applications.

In this paper, the high gain array of the antenna based on a modified dual polarised aperture coupled stacked Microstrip patch antenna is proposed. In order to combat the mentioned vital challenges in antenna design for chipless RFID tag detection, an 8×8-element array antenna with high gain, high front to back ratio (FBR), dual polarized feather and planar structure was successfully designed, fabricated and measured.

This paper is arranged as following: in Section II of this paper, the made contributions based on theory of the antenna is explained followed by the design procedure of the single element and the array antenna in section III. Section IV provides information about the effects of back reflectors. All the results of antenna measurement are demonstrated in section V. The performance of the proposed antenna in a chipless RFID system is evaluated, and the results are provided in section VI. The last section, section VII, of this paper is the conclusion.

II. THE CONTRIBUTIONS OF THIS PAPER BASED ON ANTENNA THEORY

A few original contributions are made in the design of chipless RFID reader antenna which will be explained as following:

(i) The first contribution is designing the antenna in a frequency band which is approved by FCC regulation. Therefore, the frequency bandwidth of 4.2 to 7.1 GHz was chosen for this chipless RFID system to simplify the implementation of the reader and chipless RFID tag fabrication. One advantage of selecting this frequency band is that the second harmonic frequency which can be generated in any element in the reader UWB transceiver blocks, tag and antenna are excluded from the operating bandwidth. As a result, in this bandwidth, the chipless RFID tags which contain resonators with second harmonics can also be detected without any confusion. The designed antenna yields 51.3% operational bandwidth centred at 5.65 GHz.

(ii) The second contribution of the design is that the back lobe level of the antenna has been reduced by adding two layers of reflectors: a complementary back reflector followed by a solid metallic reflector. The complementary reflector is a plus-shaped resonant structure that augments the bandwidth. The second metallic reflector is a solid reflector that reduces the back lobe significantly. The combination of the two reflectors provides UWB back lobe suppression with appropriate phase compensation over the bandwidth. The achieved front to back ratio of the antenna was 22 dBc all over the bandwidth in average.

(iii) The third contribution is that the gain of the antenna in a single element as well as in array synthesis has been increased; since the primary hypothesis of designing this antenna with high gain was chipless RFID tag detection in high ranges. It should be noticed that enhancing the reading range in a chipless RFID system depends on many factors: (1) increasing the sensitivity of reader in both microwave and digital sections, (2) improving the return loss of the reader antenna so that less reflective loss in the antenna transmit/receive chains occurs, and (3) increasing the gain of the reader antenna and finally, (4) high RCS of the chipless tag. All these factors enhance the performance of the system and increase the reading range. In a scenario in which the reader architecture is fixed, such as the developed reader by the author [5] or a complementary commercial transceiver system such as a vector network analyser (VNA), and using

a typical chipless RFID tags which has low RCS, the only solution for enhancing the performance of the system is using a high gain reader antenna. Therefore, a UWB high gain antenna with low return loss is required. The single element antenna used for this array synthesis generated 9.27 dBi gain and the 8×8-element array antenna produced 26dBi gain in measurement.

(iv) The proposed antenna is designed with two perpendicular polarisations. The dual polarised feature of this antenna is beneficial for chipless RFID tag detection when the tag designed with cross-polar RCS, or it is designed as a hybrid-polarised tag. In order to detect a cross-polar tag, the transmitter and receiver antennas are adjusted with perpendicular polarisations. Moreover, in frequency-polarisation hybrid tags, the data are embedded in the tag in two orthogonal polarisations in order to increase data capacity. Therefore, it is necessary to measure the tag frequency signature in both vertical and horizontal polarisations. As a result, the isolation between two ports of the antenna is another important parameter which affects the performance of the system. One of the great achievement of this design is having more than 48 dBc isolation between orthogonal ports in the single element and better than 32 dBc for the array antenna.

(v) The designed antenna was implemented in a chipless RFID system and the performance of the antenna for tag detection in long distance was evaluated. The antenna is capable of detecting a multi-bit chipless RFID tag for high ranges above 8 meters using a commercial VNA as a reader with a transmit power of −10 dBm. Compared with the conventional chipless RFID systems with the maximal reading range of a few centimetres, the proposed antenna has achieved a much longer reading range.

III. DESIGN PROCEDURE

In this section, the design procedure of the dual polarised UWB antenna element followed by the 8×8-element array antenna are presented. The proposed antenna is based on a modified version of the aperture coupled stacked microstrip patch antenna, arranged in an array design with a uniform excitation.

A. SINGLE ELEMENT

The single element antenna configuration consists of six interleaved layers as shown in Fig. 2. The first two top layers consist of the parasitic and exciting square Microstrip patch antennas, respectively, with an air gap (h_1) to enhance the operational bandwidth. The next layer is a proximity coupled feed line (with air gap h_2 from the bottom exciting patch substrate) with a U-shaped T-junction power divider with two 100 Ω output branches and a 50 Ω feed line. This bifurcated proximity coupled feed line excites the bottom patch antenna as is designated as Port#1. The next bottom layer is a ground layer with a cross-slot coupling aperture. The coupling aperture of the ground plane is designed to couple the exciting patch with the second feed network with the perpendicular polarisation compared to the Port#1 feed.

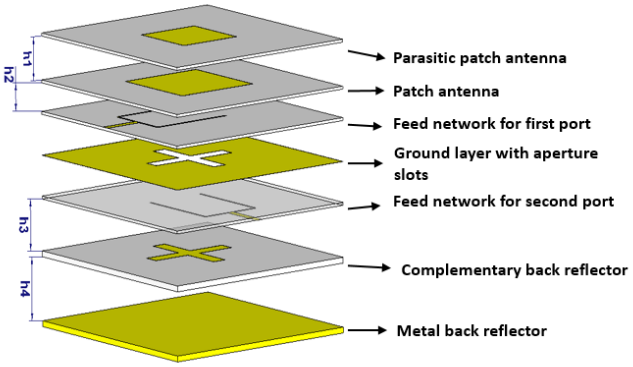

FIGURE 2. Single antenna structure.

The two feed networks in different layers maximise the isolation between the two feed ports. The feed network of the second port has the same configuration as the first port, but it has a ground plate with slots on the top layer and the feed network layer at the bottom, as shown in shown in Fig. 2. The feed network for Port#1 and Port #2 have a common ground plate with a similar design and the only difference between them is 90 degrees rotation between them for producing a perpendicular polarisation at each port.

The fifth layer of this structure is a complementary reflector with the same shape and size of the cross-shaped coupling slots. This complementary reflector is used for enhancing the bandwidth and reducing the back lobe level. Moreover, the last piece of this design is a solid metal layer used as a back reflector to improve the front to back ratio and reduce the sensitivity of the antenna to the environment in chipless RFID applications.

For this structure, there are four air gaps as designated as h1 to h4 in Fig. 2. The gap between the exciting and parasitic patch improves the bandwidth, and the air gaps below the feed network are required to reduce back lobe level.

The substrate for the first four layers of this antenna design is TLX-8 with a dielectric constant of 2.45 and a thickness of 0.5 mm. The last two reflector layers were designed on FR-4 substrate with dielectric constant of 4.3 and a thickness of 1 mm to reduce the cost of the antenna.

B. ARRAY SYNTHESIS

In many applications based on the requirements of high gain and directive pattern for long distance communication, it is necessary to design the antenna array. The single elements usually have a low gain with wide beamwidth [7]. The antenna array arrangement can be in 1D linear, 2D, circular or non-uniform arrangement. The excitement coefficients and distance between elements are the main factors which shape the array radiation pattern. The total radiation pattern is a multiplication of the radiation pattern of the single component and the array factor.

$$E\,(total) = [E\,(single\ element\ at\ refrence\ point)] \times [arry\ factor] \quad (1)$$

In the case that the inter-element spacing is $\geq \lambda$, multiple maxima, which are called as grating lobes, will occur [8]. By utilising the designed single element and implementing the array synthesis theory, an 8×8-element array with ultra-wide bandwidth and the high gain was synthesised. The arrangement of this array antenna is symmetric with uniform excitation. The spacing between each element in all rows and columns are 43 mm which is equal to 0.8λ at 5.65 GHz.

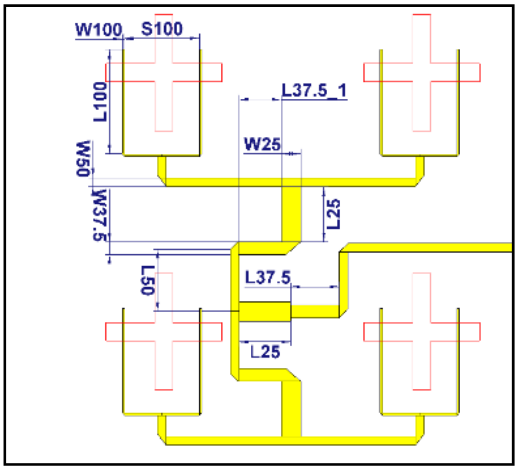

FIGURE 3. A 1 to 8-way power divider as a unit cell of feed network structure.

C. BEAMFORMING FEED NETWORK

The unit cell for designing the power divider in the feed network is shown in Fig. 3. It is a corporate feed 1- to-8-way T-junction power divider on Microstrip structure by the presence of cross-shaped slots in the ground plane. As mentioned, each antenna element is excited by an each of 100 Ω U-shaped feed lines are connected to 50 Ω line. In order to combine two antenna input ports, each pair of 50 Ω feed lines were combined using three stages of T-junction power divider with 25, 37.5, and 50 Ω. The $\frac{\lambda}{4}$ transformers designed at the center frequency of 5.65 GHz. A similar ultra-wideband power divider with three stages was used for combing all 50 Ω lines. Since the spacing between each element in the array was limited, in order to implement a line with a length of $\frac{\lambda}{4}$, folding techniques with optimiztion were used to fit the strcuture in the specific area.

In order to implement the uniform excitation of the array antenna a UWB 1-to-128-way power divider with the presence of cross-shaped slots was designed as it is shown in Fig. 4 (a) and (b), the design of the top and bottom layer of feed network, respectively. As it can be seen to combine the power from each 1-to-8-way power divider, the similar structure of power divider with three stages was used. The coupling effect of adjacent feed lines, the impact of the coupling slots and filling a three-stage power divider in the available space between elements were the main challenge in designing the feed network. This requires enormous design optimisation to reduce the adverse coupling effect and achieve the best return loss and isolation between feed ports. A similar

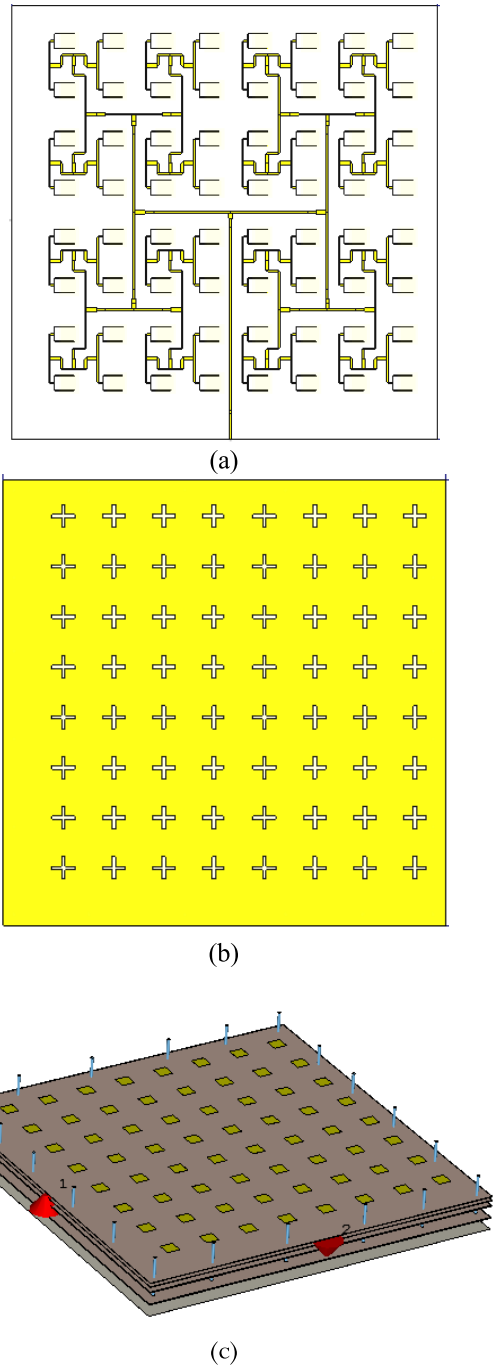

FIGURE 4. The array antenna (a) the top layer of the feed network, (b) the bottom layer of the feed network (ground with cross-shaped slots), and (c) the array structure.

structure of feed network was used for the second port of the antenna with a perpendicular polarisation as explained in the single element design. A perspective view of the array antenna is shown in Fig. 4 (c). The total size of this antenna is 38 cm × 38 cm.

Similar to the single element design, the first four layers of this antenna array were designed on Taconic TLX-8 substrate with 0.5 mm thickness, and last two layers at the bottom were designed on FR-4 with 1 mm thickness, to reduce the cost.

IV. THE EFFECT OF THE BACK REFLECTORS

The back lobe is an inherent problem for the UWB aperture coupled patch antenna. The back lobe occurs because the coupling aperture on the ground plane also needs to resonate nearby frequency of the patch radiator to increase the bandwidth. Thus, the aperture is also radiating in both front and back direction equally. In this case, almost half of the power is wasted in the back lobe, which is inconvenient for chipless RFID applications. The main lobe of the antenna should only interact with a tag for large reading range, and suppression of interference and noise from the environment. Therefore, two back reflectors were added to the design. The first layer is a complementary back reflector, which is used for enhancing bandwidth and reducing the back lobe level, the second metallic back reflector improves the F/B ratio significantly. The spacing between the feed network and the complementary back reflector is the same spacing between two back reflectors which should be $\frac{\lambda}{4}$ in theory. However, for a UWB antenna, this spacing was optimised in CST Microwave Studio to have an acceptable return loss and an excellent front to back level at the same time. The optimal achieved spacing was 0.24 λ at the center frequency. The optimized results are produced in section IV Results.

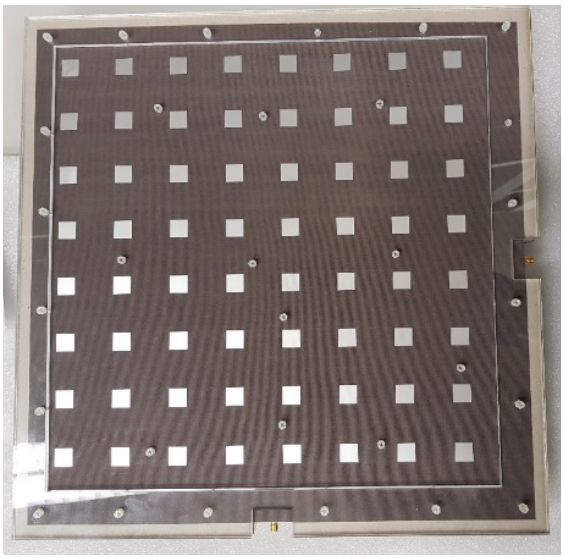

FIGURE 5. The assembled antenna array of 8by8 elements.

Finally, the 8×8-element interleaved array antenna is fabricated using photolithograph chemical etching and assembled with spacers between the layers. Fig. 5 shows the photograph of the assembled antenna. The physical size of these antennas including the support jigs is 40 cm× 40 cm ×10 cm. The antenna was used to measure a 4-bit chipless tag RFID tag at long ranges. The utilised tag was developed in Monash Microwave, Antenna, Radio-Frequency and Sensor (MMAR) lab and presented in [9].

V. RESULTS

This section presents the CST Microwave Studio simulation and measured results of the 8×8-element array. Due to the space limitation of the paper, the results for the single elements is not produced here except the S-parameters and a sample of the radiation pattern.

A. SINGLE ELEMENT

1) S-PARAMETERS

The S-parameters of the single antenna in the simulation is shown in Fig. 6. In this structure, the excitation of port #1 is coupling between the feed network with the stacked patch antenna and via port #2 excite the antenna with aperture couple techniques. As it can be seen in this figure, the return loss at port #1 has a higher value as compared to port #2. The frequency bandwidth of this antenna is 4.4 to 7.9 GHz and 4.89 to 7.95 GHz for the first and second ports respectively. Moreover, the isolation between two ports is higher than 49 dBc.

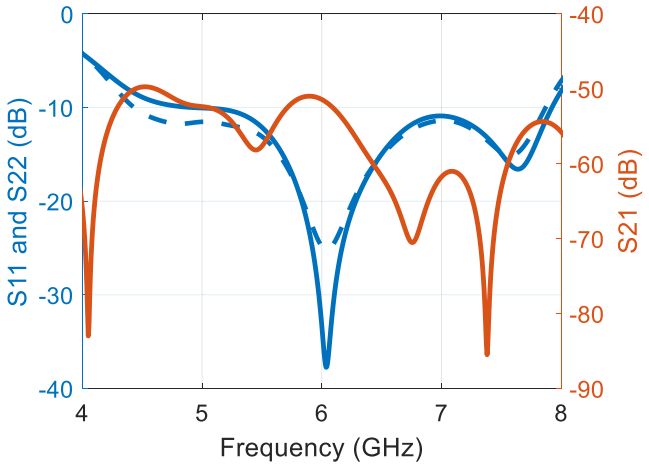

FIGURE 6. S-parameters of the single element, S11 (blue - - line), S22 (blue line) and S21 (red lines).

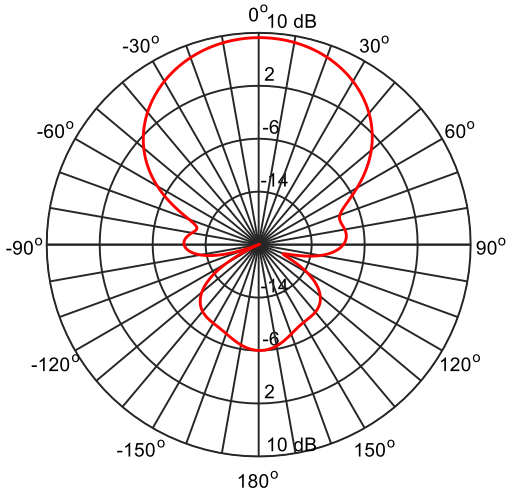

FIGURE 7. E-plane Radiation pattern of a single element antenna at 6 GHz.

2) RADIATION PATTERN

The radiation pattern of a single element antenna at 6GHz is demonstrated in Fig.7. As it can be seen, the maximum realised gain is 9.27 dBi. The back lobe level was less

than −15dBc and the 3 dB angular width was 63.4 degrees. In addition, the side lobe level was less than −20dBc.

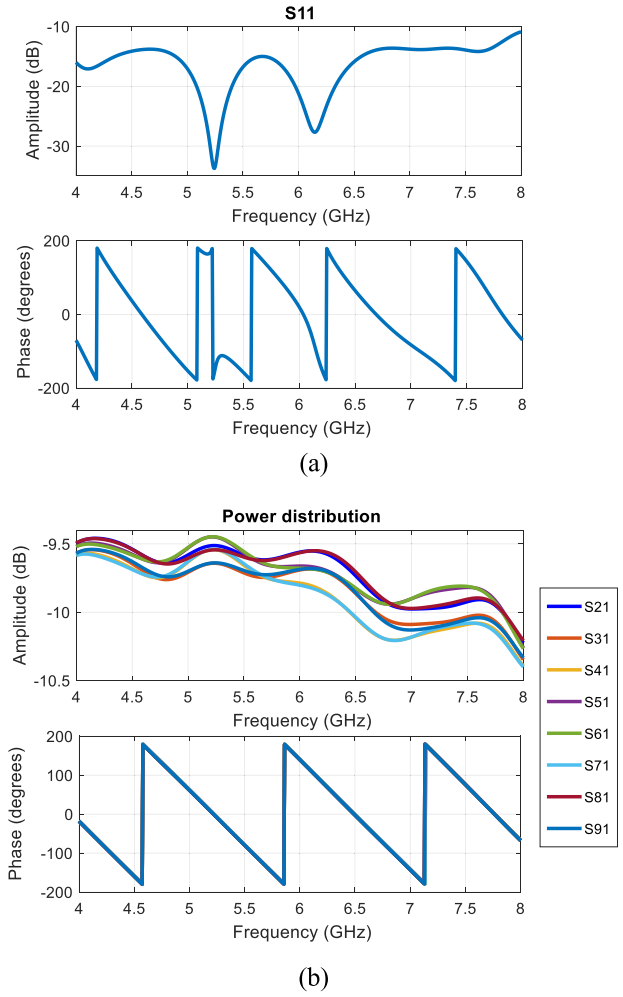

FIGURE 8. The simulation results of return loss and power distribution of a 1 to 8 power divider, (a) S11, and (b) S21, S31, S41, S51, S61, S71, S81, and S91.

B. 1 TO 8-WAY POWER DIVIDER

In this section, the simulation results of 1 to 8-way power divider are presented and discussed. The amplitude and phase of the return loss are demonstrated in Fig.8 (a). As it can be seen, the S11 of this UWB power divider is below −11dB from 4 to 8 GHz and there is a phase variation in dominant resonance frequencies. The power distribution ratios between 8 ports of this power divider are shown in Fig.8 (b). As it can be seen, due to special compact design and coupling effect between feed lines, there is an amplitude imbalance of maximum ±0.14 dB at each frequency, while there is no phase imbalance between ports. In addition, over frequency, the amplitude variation ranges from −9.4 dB at lowest frequency to −10.4dB at the highest frequency.

The 1 to 64 way power divider was designed based on modification of 1 to 8 way power divider by adding two more stages of power dividers, and at the end the 100-ohm U-shaped power, dividers were added at each port for excitation of each patch antenna in the array (the structure is shown in Fig.4 (a)).

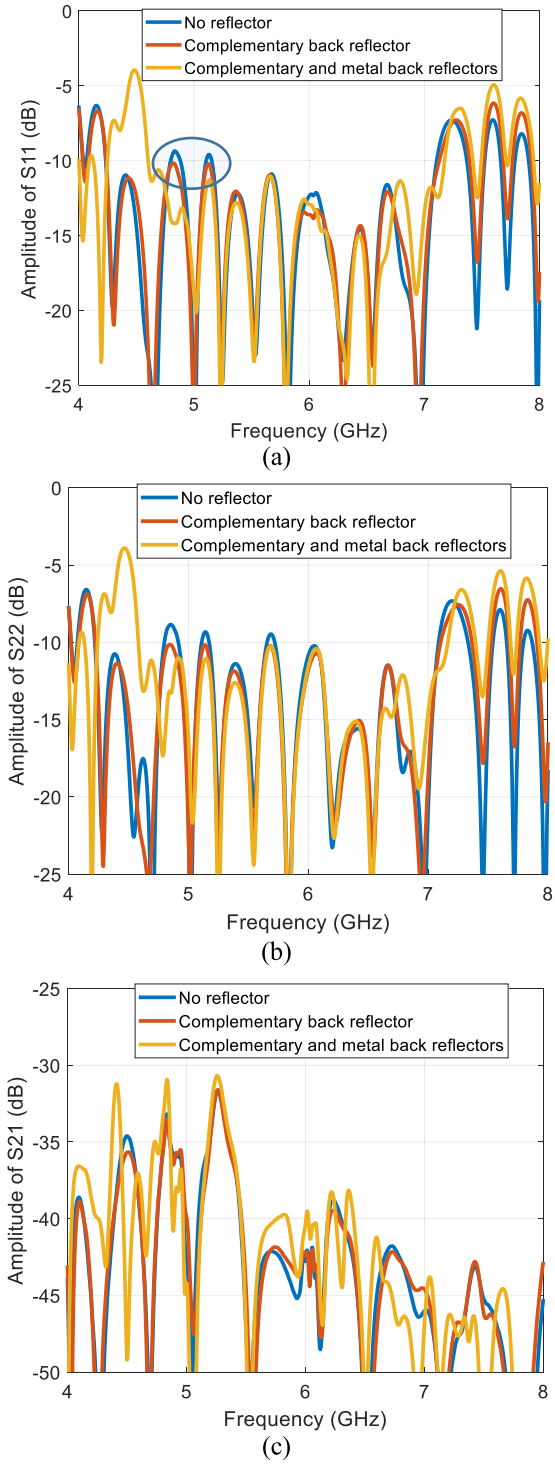

FIGURE 9. The comparison between S-Parameters with and without the presence of a metal back reflector.

C. STUDY OF BACK_REFLECTORS IN ANTENNA ARRAY

1) RETURN LOSS

The simulation results for S-parameters before and after including each back reflector are shown in Fig. 9.

By comparing the S_{ii} in three different conditions (Fig. 9 (a) and (b)), it can be seen that the complementary reflector enhances the return loss at 4.2 to 6.2 GHz by suppressing the peaks in S_{11} and S_{22}. The effect of this reflector in S_{22} is more significant as the commentary reflector is precisely below the feed network related to the second port. So, the coupling effect has a positive effect in the mid-band response. Also, there is a slight difference at a higher frequency around 6.7 GHz and caused the 50MHz bandwidth enhancement. However, the bandwidth has been reduced from the lower band frequency at 4.6 GHz. The back reflector had a similar effect on return loss at both ports. Moreover, in Fig. 9 (c), it is demonstrated that the back reflector had a slight impact on the isolation between ports. The pattern of S_{21} over frequency in presence and absence of the back reflectors were slightly different while the average values are almost the same.

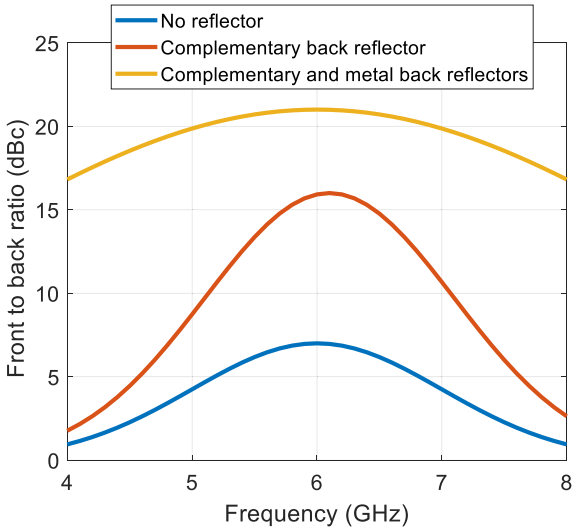

FIGURE 10. Comparison of front to back ration with presence and absence of a back reflector at port1.

2) F/B RATIO ENHANCEMENT

The more important parameter which is required to be investigated is the F/B ratio after attaching the back reflector. Fig. 10 demonstrates a comparison between the FBR in the presence and absence of the complementary back reflector and the solid back reflector at port #1. It can be seen that in the absence of both reflectors, the FBR is less than 6 dBc over the operating bandwidth while the pattern of front to back ratio with only complementary back reflector has just one peak at 6.2 GHz with 16dBc value and low values at other frequency bands. The reason behind this is that the additional back reflector could improve the front to back ratio just at 6.2 GHz as the spacing between the complementary back reflector and feed network layer are $\frac{\lambda}{4}$ at 6.2 GHz. Furthermore, by using the second layer of back reflector, the FBR has been improved all over the frequency band with an average of 17.7 dBc. The maximum value for FBR is 22 dBc at the frequency band of 5.8 to 6.2 GHz.

3) RADIATION PATTERNS

Moreover, the effect of the back reflectors can be studied in the radiation pattern. As an example, the E-plane radiation pattern at 5 GHz in both cases (with and without a metal back reflector) are plotted in Fig. 11. It is illustrating that the radiation at back side has been reduced significantly while the at front lobes the radiation patterns are still the same. So, as a conclusion of the study of the effect of the metal back reflector, this technique improved the back lobe level reduction significantly while its effect on return loss of the antenna reduces the operating bandwidth. Moreover, the recommendation is that based on the application the reflector can be added or removed in fabricated design.

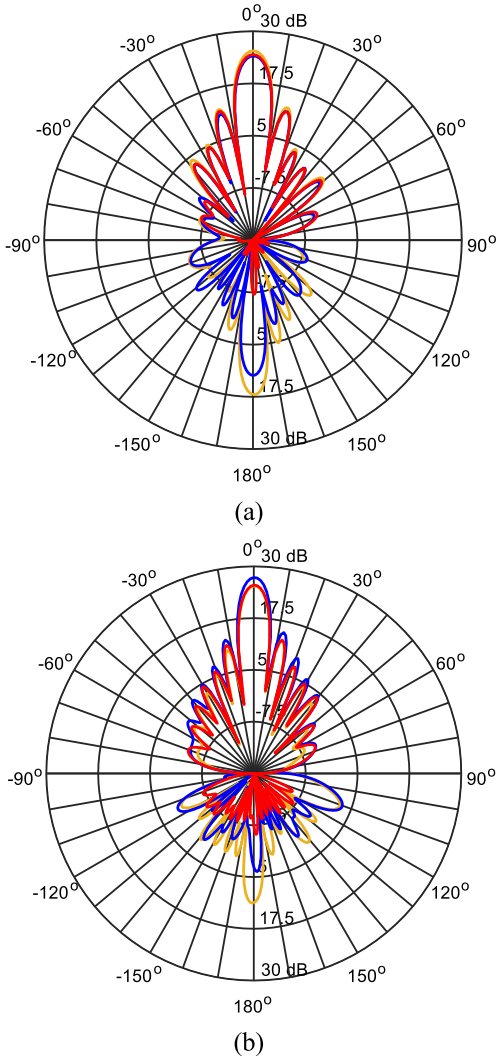

FIGURE 11. Comparison between E-plane radiation in the cases of No reflector (yellow line), the presence of only complementary reflector (blue line) and presence of both complementary and metal back reflectors (red line) at (a) 5GHz and (b) 6GHz.

According to the radiation pattern shown in Fig. 11 (a), the 3dB angular beam width in all three conditions are 8.8°, and the side lobe level is −13dB. The maximum gain in the absence of both back reflectors, the presence of the

complementary reflector, and both reflectors are 24.1, 25.3 and 24.4 dBi respectively. The pattern of the antenna is symmetrical in both E- and H-planes. The reason for a slight difference in right and left sides of the radiation pattern in Fig. 10 is due to the coupling effect between adjacent feed lines in the feed network.

D. MEASURED RESULTS OF ARRAY ANTENNA

After achieving satisfactory simulation performance, the antenna was assembled and tested in Monash Microwave, Antenna, RFID and Sensor (MMARS) laboratory. Measurements include S-parameters vs frequency using a VNA, gain vs frequency and, radiation patterns in MMARS anechoic chamber, and finally, field trials of a 4-bit chipless RFID tag detection. The procedure of measurement of each parameter and the results are given in below sections.

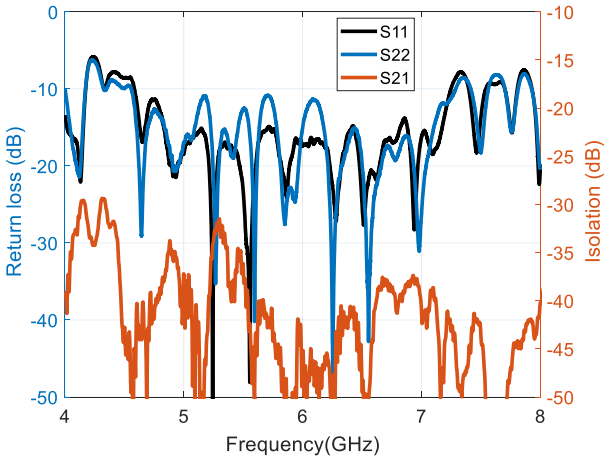

FIGURE 12. Measured S-parameters of the array antenna.

1) RETURN LOSS

In order to evaluate the performance of the antenna structures, the S-parameters at all ports were measured using analyser VNA in a lab environment. The measured return loss (S_{11} and S_{22} in dB vs frequency) and isolation (S_{21} in dB vs frequency) at both ports are shown in Fig. 12. The operating bandwidth of the array of the antenna is from 4.5 to 7.2 GHz considering S_{11} and S_{22} below -10 dB, in the presence of both back reflectors. It can be seen that the matching at port 1 is much better than port 2 in the middle band. The Maximum peak of return loss for port 1 is less than -15 dB while this value is less than -10 for the second port. Moreover, the measured isolation between two ports for this antenna is more than 32 dBc in the operating frequency band, the average value it is around 40 dBc.

2) GAIN BANDWIDTH

The gain of the 8x8-element array antenna was measured using a signal generator and a spectrum analyser in Monash University aniconic chamber. The first step was measuring the maximum gain over frequency which is related to co-polar radiation pattern at 0 degrees angle in front of the antenna. The measurement was done using a 10 dBi gain UWB horn antenna. The transmitted power was 10 dBm, and the distance between horn antenna the array antenna was 3.4 meters. The total cable loss was measured at frequency bandwidth of 3.5 to 9 GHz and subtracted from the received power to calculate the absolute gain.

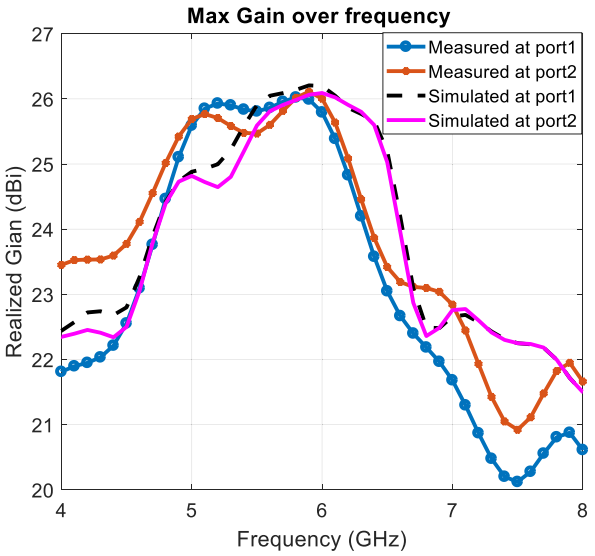

FIGURE 13. Comparison between maximum gain over frequency in simulation and measurement at both ports.

The simulated and measured maximum gain in dBi vs frequency are shown in Fig. 13. The two sets of data are in good agreement with a maximum 26 dBi gain at both ports. The 3dB gain bandwidth span is at 3.8 GHz to 7 GHz. The 3dB gain bandwidth at port two is wider than the bandwidth defined by return loss. The slight discrepancies between the two sets of data can be attributed to the fabrication tolerance and assembly errors.

3) RADIATION PATTERN

After obtaining a satisfactory gain bandwidth, the co-polar and cross-polar radiation patterns in E-plane and H-plane for both ports are measured. Fig. 14 shows the simulation and measured radiation patterns at 5GHz and 6 GHz.

It can be seen that the measured results at both frequencies are similar to the simulated one with slight discrepancies due to the aforementioned errors. In E-plane co-polar radiation patterns, the 3-dB beamwidth is 8 degrees in simulation and 5 degrees in measurements. The measured side love level was more than 12 dBc at all frequency points. Similarly, in H-plane co-polar radiation pattern, the side lobe level are less than 13 dBc at both frequencies.

Furthermore, the cross-polar E-field at all mentioned frequency points were measured by setting the transmitter and receiver antenna with a perpendicular polarisation, which is shown in Fig. 14 with yellow lines. In the E-plane radiation patterns, the measured cross-polar value is less than -5dBi which means -31 dBc less than the co-polar value

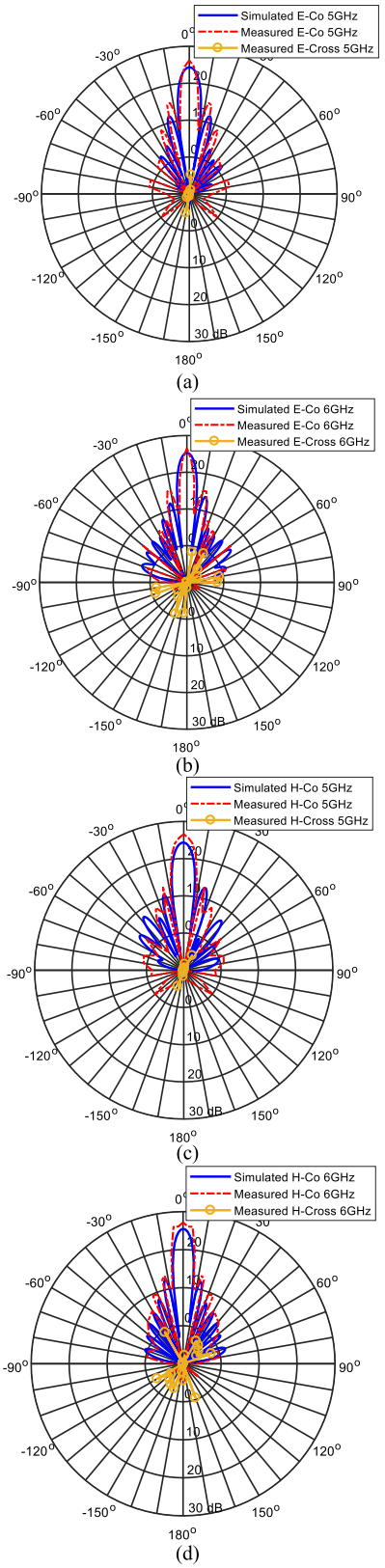

FIGURE 14. The simulated and measured results of co-polar and cross-polar radiation pattern in E and H plane (a) E-plane at 5GHz (b) E-plane at 6GHz, (c) H-plane at 5GHz, (d) H-plane at 6GHz.

approximately. Similarly, in the H-plane radiation pattern the measured cross-polar value is less than −10 which means at least 26 dBc less than the co-polar value in H-plane at both frequency points.

Moreover, the information related to measured radiation pattern at other frequencies at co-polar and cross-polar are shown in Table.1. For each port, the main lobe level and side lobe in the co-polar and maximum value of cross-polar in both E-plane and H-plane were calculated and reported in this table.

As the significant information at both ports, it can be seen that at 4 GHz the maximum co-polar gain in all plane is 23 dBi with 12 dBc sidelobe level and the cross-polar value is 23dBc less than the co-polar value. Moreover, at 5 GHz, the maximum co-polar gain is 26 GHz with side lobe level less that −12dBc, and the cross-polar value is between −27 to 33.5 dBc.

Similarly, at 6 GHz the maximum co-polar value is 26.5 with 13 dBc sidelobe level and less than −27 dBc cross-polar value. Also, at 7 GHz, the maximum co-polar gain is 24dBi with less than −12 dBc sidelobe level and less than −23 dBc cross-polar value.

VI. CHIPLESS RFID TAG DETECTION

After successful design, fabrication and testing of the array antenna, the antenna is deployed in chipless RFID field trails. Please note that we use only one polarisation to measure the tag response. The antenna can be used for measurement of high data density tags with dual by using two perpendicular ports of the antenna. Fig. 15 shows the photograph of the measurements set up. The measurement of tag detection is done in a noisy laboratory environment to investigate the robust performance of the antenna used.

The operating frequency band of this antenna is from 4.5 to 7.3 GHz in the presence of both reflectors. Based on the formula for calculating the maximum distance for tag detection [10].

$$R^{max} = \sqrt[4]{P_{tx} \cdot G_{tx} \cdot G_{rx} \cdot \frac{\lambda^2}{(4.\pi)^3 \cdot P_{rx}^{min}} \cdot \sigma_{min}} \qquad (2)$$

where, P_{tx} is the transmitting power, G_{tx} and G_{rx} are gain of transmitting and receiving antennas, σ_{min} is the minimum level of RCS which can be detected, and P_{rx}^{min} is the receiver sensitivity. The sensitivity of the reader (VNA) can be considered as the noise level of the system or 10 dB above the noise level. Using the array antenna with 26 dBi gain, −10 dBm transmitting power and −80 dBm sensitivity of reader and minimum RCS −23 dBsm of the tag at 5 GHz, the expected maximum distance for detection of this tag is 10.95m.

In order to test the performance of this antenna in chipless RFID system, a system setup including an Anritsu VNA 37247D as a reader, a hexagonal shaped chipless RFID tag [9], and the antenna, was used as shown in Fig. 13. The utilised tag is a broadband chipless RFID tag operated by 3-10 GHz, and it includes three resonances in the antenna frequency band. In this measurement, the tag response was

TABLE 1. The information related to radiation pattern at both ports.

Frequency (GHz)	Port1						Port2					
	Co-polar				Cross-polar		Co-polar				Cross-polar	
	*EP**		*HP***		EP	HP	EP		HP		EP	HP
	*ML****	*SL*****	ML	SL	ML	ML	ML	SL	ML	SL	ML	ML
4	23	12	23	12	-25	-23	23	12	23	12	-23	-23
5	25.5	12	26	14	-30.5	-33.5	26	12	25.5	13	-28	-27
6	26.5	13	26.5	13	-33.5	-26.5	26.7	12	26	12	-27.6	-27
7	23.5	15	24	12	-27.5	-25	23	14	23	12	-24	-23

*E-plane
** H-plane
***Main lobe level (dBi)
**** Sidelobe level (dBc)

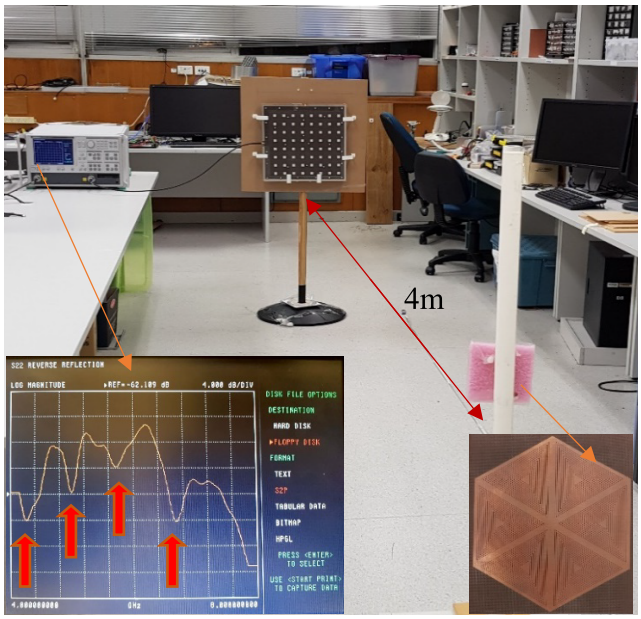

FIGURE 15. Chipless RFID tag detection setup using the antenna.

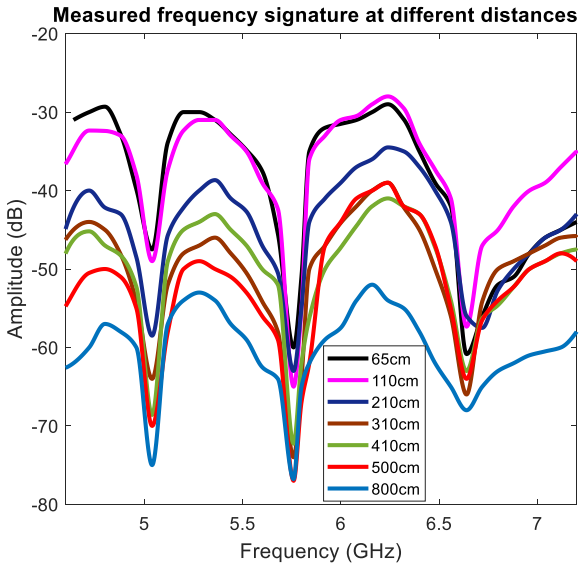

FIGURE 16. Measured frequency signature of a chipless RFID tag at different distances from the reader antenna.

measured in a frequency range of 4 to 8 GHz, and the results are demonstrated in a frequency- range of 4.5 to 7.2 GHz.

For the tag frequency signature, measurement a single antenna technique was used. In addition, the background subtraction was also utilized for measuring the resonance pattern. To do that, the antenna was connected to the reader and the $S_{11}(no\ tag)$ was measured in absence of the tag, then after placing the tag in front of the antenna the $S_{11}(tag)$ was measured. The frequency signature can be extracted by subtracting these two values as

$$\Delta S_{11} = S_{11}\,(tag) - S_{11}(no\ tag) \tag{3}$$

The frequency signature of the tag measured at different distances from the reader antenna is shown in Fig. 16. In this figure, the selected frequency range is from 4.5 to 7.2 GHz, which includes three resonances. In can be seen that the frequency signature at 65 cm to 8 m has a similar pattern and only the level of the signal has been reduced over distance due to free space loss effect. It should be noticed that due to the limited space in the lab, the tag frequency signature were measured up to 8m and based on the theoretical calculation the range can be longer. This result proves the excellent performance of this antenna in chipless RFID tag detection.

VII. CONCLUSIONS

In this paper, a high gain dual polarized ultra-wideband antenna with aperture coupled microstrip patch antenna for enhancing the reading range in chipless RFID application is proposed. This structure is planar with high front to back ration all over the bandwidth. The operating frequency of this antenna is 4.2 to 7.1 GHz in the absence of the metal back reflector and 4.5 to 7.2 GHz in the presence of both reflectors.

Moreover, the maximum realised a gain of 26 dBi at both ports. The isolation between two ports is more than 32 dB. A complementary back reflector and metal plate back reflector were used to reduce the back lobe level significantly. The measured returned loss, isolation, gain, and radiation pattern met the simulation results. The antenna was tested in chipless RFID application in a signature could be detected in the distance above 8 m. The laboratory environment, and the tag measurement results for chipless RFID tag detection proved the excellent performance of this antenna in enhancing the reading zone in chipless RFID applications.

REFERENCES

[1] S. Preradovic and N. C. Karmakar, "Chipless RFID: Bar code of the future," *IEEE Microw. Mag.*, vol. 11, no. 7, pp. 87–97, Dec. 2010.
[2] A. Vena, E. Perret, and S. Tedjini, "Chipless RFID tag using hybrid coding technique," *IEEE Trans. Microw. Theory Techn.*, vol. 59, no. 12, pp. 3356–3364, Dec. 2011.
[3] S. Preradovic and N. C. Karmakar, *Multiresonator-Based Chipless RFID: Barcode of the Future*. New York, NY, USA: Springer, 2012.
[4] S. Preradovic, "Chipless RFID system for barcode replacement," Ph.D. dissertation, Elect. Comput. Syst. Eng., Monash Univ., Melbourne, VIC, Australia, 2010.
[5] N. C. Karmakar, *Chipless RFID Reader Architecture*. Boston, MA, USA: Artech House, 2013.
[6] M. A. Islam, "Compact printable chipless RFID systems," Ph.D. dissertation, Elect. Comput. Syst. Eng., Monash Univ., Melbourne, VIC, Australia, 2014.
[7] C. A. Balanis, *Antenna Theory: Analysis and Design*, 3rd ed. Hoboken, NJ, USA: Wiley, 2005.
[8] M. Zomorrodi and N. C. Karmakar, "On the application of the EM-imaging for chipless RFID tags," *Wireless Power Transf.*, vol. 2, pp. 86–96, Sep. 2015.
[9] M. A. Islam, Y. Yap, and N. Karmakar, "'Δ' slotted compact printable orientation insensitive chipless RFID tag for long range applications," in *Proc. Int. Conf. Elect. Comput. Eng. (ICECE)*, Dec. 2016, pp. 283–286.
[10] A. Vena *et al.*, "Design and realization of stretchable sewn chipless RFID tags and sensors for wearable applications," in *Proc. IEEE Int. Conf. RFID (RFID)*, Apr./May 2013, pp. 176–183.

FATEMEH BABAEIAN (S'16) received the B.S. degree in electrical engineering from Shiraz University, Shiraz, Iran, in 2010, and the M.S. degree in electrical engineering (telecommunication) from the Amirkabir University of Technology, Tehran, Iran, in 2013. She is currently pursuing the Ph.D. degree in electrical engineering with Monash University, Australia. Her research interests include chipless RFID, microwave, antenna array synthesis, and signal processing.

NEMAI CHANDRA KARMAKAR (S'91–M'91–SM'99) received the M.Sc. degree in electrical engineering from the University of Saskatchewan, Saskatoon, SK, Canada, in 1991, and the Ph.D. degree from the University of Queensland, Brisbane, QLD, Australia, in 1999. He has over 20 years of teaching, design, and development experience in antennas, microwave active and passive circuits, and RFIDs in Canada, Australia, and Singapore. He is currently an Associate Professor with the Department of Electrical and Computer Systems Engineering, Monash University, Melbourne, VIC, Australia. He has authored or co-authored over 220 referred journal and conference papers, 24 book chapters, and eight books. He holds nine international patent applications on chipless RFID.